

A Strategy to Reduce Blocky Pattern and Contrast Loss in Emission Tomography Reconstruction with Reduced Angular Sampling and Total Variation Minimization

Jungah Son, Soo Mee Kim and Jae Sung Lee

Received: 20 December 2014 / Accepted: 24 December 2014

© The Korean Society of Medical & Biological Engineering and Springer 2014

Abstract

Purpose Reducing radiation dose or scanning time is important for patient safety when using nuclear medicine technique. The aim of this study is to develop a reconstruction method to suppress deterioration of image quality with only a small sampling number of projection data in single photon emission computed tomography (SPECT).

Methods We used total variation (TV) image reconstruction. However, the images reconstructed using expectation maximization (EM)-TV show systematic loss of contrast and blocky artifacts when the measurement data is noisy like SPECT data. Therefore, we first reduced projection data noise using a combination of diffusion filters and then reconstructed images from noise-reduced sinogram. Perona-Malik (PM) anisotropic diffusion filter and the nonlinear geometric diffusion filter were combined.

Results For both the 3D Torso phantom and the NEMA IEC phantom, systematic contrast loss was seen when the images were reconstructed using EM-TV. In the Torso phantom, the combined filter showed similar normalized mean square error, streak indicator, and beta values to PM filter, but the signal-to-noise ratio gain of the image was the highest using the combined filter. In the NEMA phantom, background variability was considerably reduced when the combined

filter was applied as pre-filters. Compared to geometric-EM-TV, combined-EM-TV preserved edges well and produced a high-contrast image.

Conclusions EM-TV with the combination of PM and geometric nonlinear diffusion filters was found to improve uniformity while maintaining contrast-to-noise ratio when angular sampling is low. The TV image reconstruction combined with the proposed diffusion filter can be beneficial for clinical SPECT imaging.

Keywords Single photon emission computed tomography (SPECT), Anisotropic diffusion, Geometric nonlinear diffusion, Total variation (TV) image reconstruction

INTRODUCTION

Single photon emission computed tomography (SPECT) imaging allows us to visualize functional information associated with various pathologic conditions. Since SPECT scans are less expensive than positron emission tomography (PET) scans, they are widely used in spite of their relatively low sensitivity and poor spatial resolution. For imaging modalities used in nuclear medicine including SPECT, increasing scanning time is closely related to the image quality improvement. Nonetheless, the long scan time can cause patient movements which produces distortion of the images and loss of effective spatial resolution. In some pediatric studies that require long scan time (i.e. basal/acetazolamide stress brain perfusion SPECT study) [1], therefore sedation or anesthesia is necessary to minimize the artifacts related to the patient movement. SPECT scan time can be shortened by reducing the angular samples of projection data. However, reducing angular sampling is accompanied by deterioration of the reconstructed image quality. In medical imaging society,

Jungah Son, Jae Sung Lee (✉)
Department of Nuclear Medicine, Seoul National University College of
Medicine 28 Yungun-Dong, Chongno-Gu, Seoul 110-744, Korea
Tel : +82-2-2072-2938 / Fax : +82-2-745-2938
E-mail : jaes@snu.ac.kr

Soo Mee Kim
Department of Radiology, University of Washington, Seattle, Washington,
USA

Jae Sung Lee
Institute of Radiation Medicine, Medical Research Center, Seoul National
University, Seoul, Korea

many attempts have been made to maintain image quality even with only a small sampling number of projection data [2-8]. Total variation (TV) image reconstruction, which was first introduced for computed tomography (CT) reconstruction, is one way of reducing artifacts originated from reducing angular sampling [9]. It is a method based on the fact that medical images are sparse in the gradient magnitude domain [9], and this method was also shown to be effective in reducing gap artifacts during PET image reconstruction [10].

The aim of this study was to minimize the SPECT angular samples by means of a TV minimization algorithm. However, the main technical challenge in TV reconstruction of SPECT data is that the SPECT projection data is much noisier compared to the data in CT, and TV image reconstruction is problematic when the measurement data is too noisy. Systematic loss of contrast and blocky patterns are typically yielded when TV image reconstruction is applied to noisy low angular sampled data [10].

Therefore, when reconstructing SPECT images using TV minimization algorithm, some noise reduction methods need to be applied to SPECT projection data beforehand. To reduce noise, several types of diffusion filters have been proposed. A geometric nonlinear diffusion filter [11] was proposed as a solution to the fast noise reduction in low-dose x-ray imaging. Although it was effective in reducing impulse noise, it could not preserve edges very well compared to the Perona-Malik (PM) diffusion filter, which is based on the gradient-dependent diffusivity function [12]. On the other hand, the PM diffusion filter cannot distinguish between edges and noise, which leaves some noise. For the above reasons, in this study, we propose a combination of geometric nonlinear and PM diffusion filter as a way of reducing noise while preserving edges in SPECT projection data.

We simulated angular sampling reductions and compared them with full angular sampling. Normalized mean square error (NMSE), normalized streak indicator (SI), beta metric (\hat{a}) and signal to noise ratio (SNR) gain (g) were measured for digital phantom data while contrast to noise ratio (CNR) and uniformity were measured from the reconstructed images of real SPECT data.

MATERIALS AND METHODS

Noise reduction using diffusion filters for SPECT TV reconstruction

Projection data noise reduction by combining geometric and PM anisotropic diffusion filters

Perona and Malik introduced a nonlinear partial differential equation (PDE) based anisotropic diffusion [12]. The discrete update equation for a current pixel of interest p_R^t in projection data p is written as

$$p_R^{t+\Delta t} = p_R^t + \left(\frac{\lambda}{4}\right) \sum_{p \in \eta_R} c(|\nabla p|) \nabla p$$

, where p_R^t is a discrete image at time t , η_R is the spatial neighborhood of p_R^t , λ is a diffusion rate constant, and $c(\cdot)$ is an edge-stopping function defined as

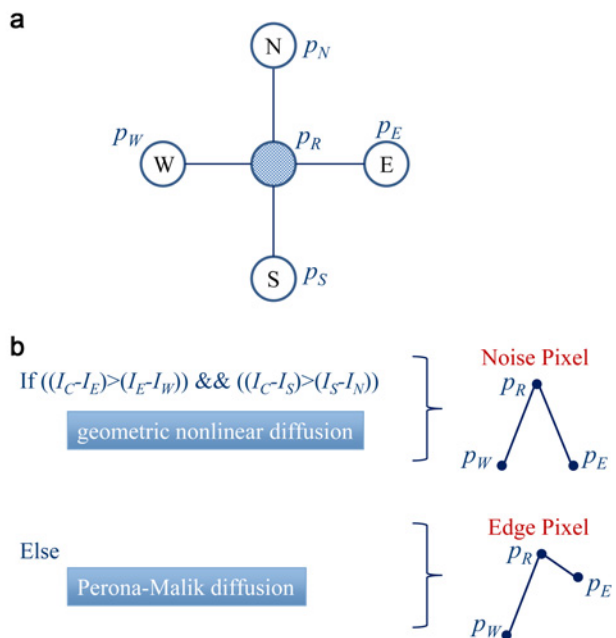


Fig. 2. (a) Four neighbors of a current pixel of interest and (b) the image corrupted by noise.

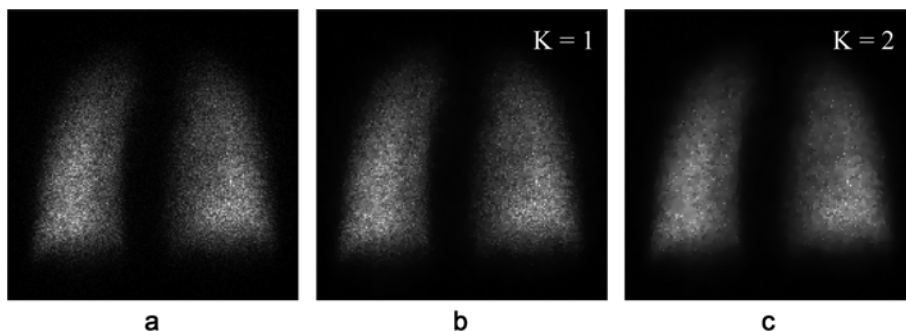


Fig. 1. Perona-Malik diffusion applied planar images when (a) original image, (b) $K = 1$ and (c) $K = 2$ obtained.

$$c(x) = \frac{1}{1 + \frac{x^2}{K^2}}$$

for a positive constant K . Fig. 1 shows planar lung ventilation images after applying Perona-Malik (PM) diffusion filter. As K gets larger, the image gets more smoothed. It can be seen that noise has been removed considerably with preserving edges. However, PM diffusion filter does not remove noises completely.

The geometric nonlinear diffusion filter [11] proved to be successful in removing the noises better than PM diffusion filter and the discrete update equation of the filter is defined as:

$$p_R^{t+\Delta t} = p_R^t + \lambda [c(D_x, P_x) \cdot (\nabla_E + \nabla_W) + c(D_y, P_y) \cdot (\nabla_N + \nabla_S)]^t$$

where ∇_p ($p = E, W, N,$ and S) represents the difference between a central pixel and one of the east, west, north, and south pixels, which are illustrated in Fig. 2a.

The parameters P_x, D_x, D_y, P_y used in above were defined as:

$$D_x = \begin{cases} |p_E - p_W| - \delta & \text{if } |p_E - p_W| > \delta \\ 0 & \text{else} \end{cases},$$

$$A_x = (p_E + p_W) / 2,$$

$$p'_{R,x} = \begin{cases} p_R - \frac{D_x}{2} & p_R > A_x \\ p_R + \frac{D_x}{2} & p_R \leq A_x \end{cases}$$

$$P_x = p'_{R,x} - A_x$$

where p_E and p_W are the image intensities at the east and west neighboring pixels, respectively. $D_y, A_y, p'_{R,y}$, and P_y are defined in the vertical direction in a similar way for the north and south neighboring pixels (p_N, p_S). δ is an auxiliary parameter to prevent small noise regions from being identified as edges.

The diffusivity functions are defined as below:

$$c(D_x, P_x) = \frac{1}{1 + (D_x/P_x)^2}$$

$$c(D_y, P_y) = \frac{1}{1 + (D_y/P_y)^2}$$

The geometric nonlinear diffusion filter uses gradient values as information to distinguish noise pixels and edge pixels. As mentioned in the introduction, in order to achieve the benefit of both filters, we used a combination of the PM anisotropic and geometric nonlinear diffusion filters for sinogram noise reduction and compared the results with

existing methods. At noise pixels, where they have much higher or lower intensity compared to surrounding pixels, we performed geometric diffusion while at pixels other than noise pixels, we performed PM diffusion. Fig. 2b illustrates the method and below is the corresponding pseudo-code for the combined diffusion:

- 1 : $\lambda_1 = 0.25; \lambda_2 = 1.5;$
- 2 : $K = 6; \delta = 1.5; a = 0.5;$
- 3 : repeat main loop (combined diffusion)
- 4 : if $(P_x > a * D_x)$ and $(P_y > a * D_y)$ then $p_R^{t+\Delta t} = p_R^t + \lambda [c(D_x, P_x) \cdot (\nabla_E + \nabla_W) + c(D_y, P_y) \cdot (\nabla_N + \nabla_S)]^t$
- 5 : else $p_R^{t+\Delta t} = p_R^t + \left(\frac{\lambda}{4}\right) \sum_{p \in \eta_R} c(|\nabla_p|) \nabla_p$
- 6 : until {stopping criteria}

λ_1 and λ_2 here serve as time steps. Small values of λ_1 and λ_2 will have less of a smoothing effect, while larger values of them will have a greater smoothing effect. a is a parameter that can be changed adaptively depending on the noisiness of projection data and we used 0.5 in this study. An optimal stopping point (number of iterations) also depends on projection data.

Total-variation image reconstruction (EM-TV)

After reducing noise in the projection domain, the images were reconstructed using the TV image reconstruction method proposed in ref. [9]. Following is a summary of the formulation of the optimization problem and separated two-step iterative method to solve the problem.

Medical images are sparse in the gradient magnitude representation, and from this information, the problem can be stated as follows: minimizing the TV of the estimated image with the constraint that the estimated image should be consistent with the measured projection data. The equation is given by,

$$\arg \min_f \|f\|_{TV} = \sum_x \sum_y |\nabla f(x, y)|,$$

$$\text{subject to } Hf = I,$$

where f is a reconstructed image, I is the filtered SPECT sinogram (reorganized filtered projection data p in the previous section), and M is the system matrix. Below is the separated two-step iterative method that Sidky and Pan proposed [9] to solve the problem.

1) The first step: Expectation maximization step

Expectation maximization (EM) updates image voxels for an iteration n as follows:

$$f_S^{(n)} = \frac{f_S^{(n-1)}}{\sum_R H_{RS}} \sum_R H_{RS} \frac{I_R}{\sum_T H_{RT} f_T^{(n-1)}}$$

where $f_S^{(n)}$ is a S^{th} voxel value of current image estimate; I_R is a measurement in the R^{th} bin; and H_{RS} is a system matrix element representing the probability that a photon emitted from a source site S would be detected in the R^{th} bin. Usually, we apply 2 or 3 EM steps for each n -th main iteration.

2) The second step: TV-steepest descent step
 The next step is to perform gradient descent to minimize the TV of the current image estimate as follows:

$$f_S^l = f_S^{l-1} - \alpha d \frac{v}{\|v\|_2}$$

where

$$v_{x,y} = \frac{\partial \|f^l\|_{TV}}{\partial f_{x,y}^l}$$

and where α is a parameter to maintain the balance between the first step and the second step and d is the change in the image due to the first step. The $l(= 0, \dots, L-1)$ is the iteration number in the TV-steepest descent step.

For the reconstruction algorithm, we chose EM because SPECT images are degraded by statistical noise. Nonetheless, other iterative algorithms can be also used in this context.

Experimental datasets and evaluation methods

The evaluation of the proposed method covers numerical simulation and real data experiments.

Numerical simulation

The convergence rate of combined filter was evaluated using 2D Shepp-Logan (SL) phantom (Fig. 3a). Fig. 3b shows noise corrupted version of Fig. 3a.

The NMSE of the filtered images with respect to the true SL phantom image was calculated as follows:

$$NMSE = \frac{\sum_{i=1}^M \sum_{j=1}^N (I(i, j) - I_T(i, j))^2}{\sum_{i=1}^M \sum_{j=1}^N (g(i, j) - I_T(i, j))^2}$$

where I and g are the filtered and original noisy images, respectively, and I_T is the true image. We measured NMSE errors of images for each loop.

In addition, 3D digital Torso phantom in Fig. 4 was used to evaluate the combined filter as a pre-filter for TV reconstruction. We performed separate 2D diffusion filtering process to projections taken from different angles before reconstruction and compared the performance of EM-TV with and without pre-filtering. As shown in Fig. 5, 50% angular sampling reduction (sparse view) from full angular sampled sinogram was simulated for the comparative evaluation.

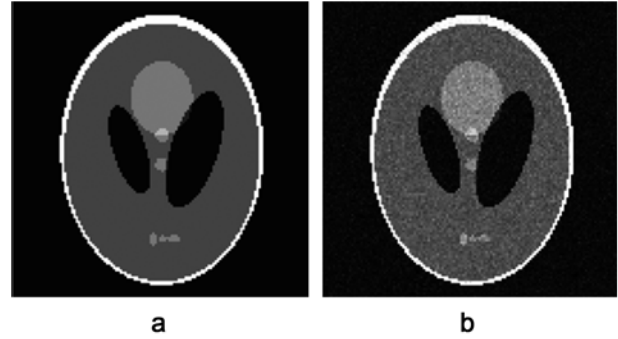


Fig. 3. (a) 2D Shepp-Logan phantom and (b) the image corrupted by noise.



Fig. 4. A trans-axial slice through the 3D digital torso phantom.

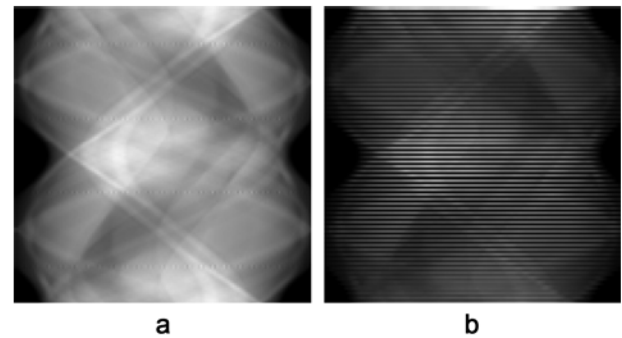


Fig. 5. (a) full angular sampled sinogram for a trans-axial slice through 3D digital torso phantom, (b) 50% angular sampling reductions.

For quantitative evaluation of the filter performances in terms of noise reduction and edge preservation, we use the metrics defined in ref. [13]. The normalized streak indicator (SI) was calculated as follows:

$$SI = \frac{abs(TV(f) - TV(f^{ref}))}{abs(TV(f^{reduced}) - TV(f^{ref}))}$$

where f is the sparse-view image reconstructed by EM-TV with filtered projections using the proposed method, f^{ref} the reference full-view image reconstructed by EM, and $f^{reduced}$ the sparse-view image reconstructed by EM-TV without pre-filtering, respectively.

To evaluate edge preservation and artifact formation, we use the beta metric (β) defined in ref. [14]:

$$\beta = \frac{D(\Delta f_{org} - \overline{\Delta f_{org}}, \Delta f - \overline{\Delta f})}{\sqrt{D(\Delta f_{org} - \overline{\Delta f_{org}}, \Delta f_{org} - \overline{\Delta f_{org}}) \cdot D(\Delta f - \overline{\Delta f}, \Delta f - \overline{\Delta f})}}$$

$$D(s_1, s_2) = \sum_{i=1}^M \sum_{j=1}^N s_1(i, j) \cdot s_2(i, j)$$

where Δf_{org} and Δf represent the edge images of the reconstructed image with original projections (f_{org}) and filtered projections (f), respectively. The edge images are calculated by applying the Canny method. $\overline{\Delta f_{org}}$ and $\overline{\Delta f}$ are the mean intensities Δf_{org} and Δf , respectively. This metric represents the resemblance of the edge images derived from the original phantom image and the reconstructed image with filtered projections.

SNR is evaluated in five different uniform-intensity circle regions-of-interest (ROIs). SNR in the ROI is defined by the mean pixel intensity divided by the standard deviation of the pixel intensity in the ROI. The SNR gain is defined by:

$$g = \frac{SNR_f}{SNR_{org}}$$

where SNR_f and SNR_{org} are the average SNRs in the reconstructed images with filtered and original projections, respectively.

Real data experiments

NEMA IEC phantom filled with ^{99m}Tc solution was scanned using a dual head SPECT (Discovery NM/CT 670, GE, USA). The concentration of the background activity in the phantom was 0.61 $\mu Ci/cc$. The spheres were filled with a concentration of 8 times as big as that of the background.

First, angular sampling reduction experiments which we did in the numerical simulation were conducted for the data acquired with 165 seconds per projection, and quantitative evaluation of percent contrast was performed.

CNR measurements were performed on the reconstructed images of the NEMA IEC phantom using all 6 spheres with

equally sized background region ROIs for each sphere. CNR was calculated by

$$CNR_j = \frac{(C_{target,j} - C_{bg})/C_{bg}}{\sigma_{bg}} \times 100\%$$

where $C_{target,j}$ and C_{bg} are the average counts in the ROI for sphere j and the average of the background ROI counts for sphere j , respectively, and σ_{bg} is the standard deviation in the background region.

The uniformity of the background ROI was calculated as follows:

$$uniformity = \left(1 - \frac{standard\ deviation\ of\ ROI}{mean\ of\ ROI}\right) \times 100\%$$

RESULTS

Numerical experiments

Convergence property of filters

Fig. 6a-c are filtered images of noise corrupted image (Fig. 3b) using PM filter ($\lambda = 1.5, K = 1$), geometric nonlinear filter ($\lambda = 0.25, \delta = 10$), and the combined filter ($\lambda = 1.5, \lambda_2 = 0.25, K = 1, \delta = 10, a = 1$), respectively. The filtered image using the combined filter restored the original image well as shown in Fig. 6c. The plot in Fig. 7 shows the NMSE change according to the number of iteration. The combined filter showed the best convergence property.

Comparison of reconstructed images of sparse view data

Fig. 8a-b show the reconstructed images using EM and EM-TV from the sparse sinogram shown in Fig. 5b without applying pre-filters. Fig. 8c-e show the images reconstructed from filtered projection data using PM filter ($\lambda = 1.0, K = 6$), geometric nonlinear filter ($\lambda = 0.25, \delta = 0$), and the combined filter ($\lambda = 1.0, \lambda_2 = 0.25, K = 1, \delta = 0, a = 2$), respectively. In the TV-steepest descent step, 10 iterations ($=L$) were used with the parameter α set to 0.1 in every step. As can be seen from Fig. 8, the image reconstructed using EM-TV shows blocky patterns mentioned in Ref. 10. The combined filter

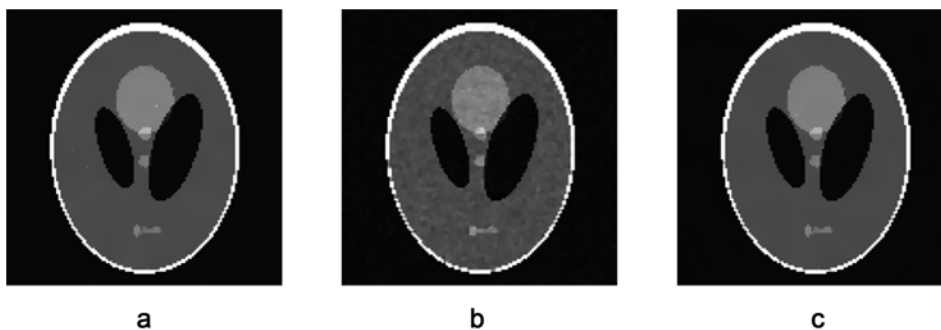


Fig. 6. Filtered images of noise corrupted image (Fig. 3b) using (a) PM filter, (b) geometric nonlinear filter, and (c) the combined filter.

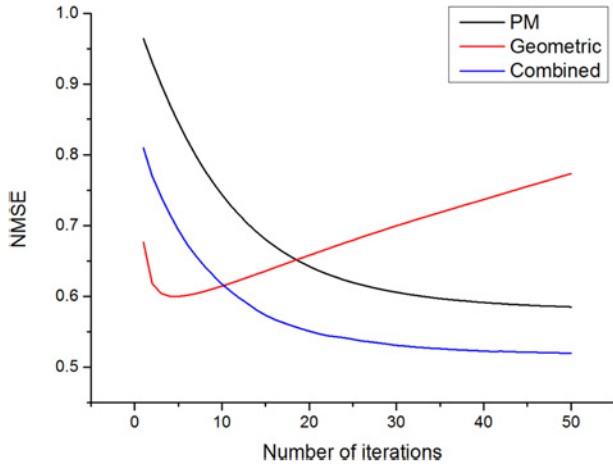


Fig. 7. Convergence of PM, geometric nonlinear, and the combined filter.

well reduced the blocky patterns while preserving edges.

Table 1 summarizes the filter performances of the three methods as a pre-filter in the case of 3D digital torso phantom. The combined filter shows NMSE, SI, and β value similar to PM filter, but the SNR gain of the image was the highest when the combined filter was used as a pre-filter.

Evaluation using real measurement data

The combined filter was tested with real SPECT images. Fig. 9 shows a slice of the reconstructed NEMA IEC phantom images of $128 \times 128 \times 128$ matrix size in transaxial view using 120 projections (full samples). The inner diameters of fillable spheres (six) were 10, 13, 17, 22, 28 and 37 mm. Fig. 10a-e show the images reconstructed from the sparse view data with 50% angular samples (60 projections) using EM, EM-TV, PM-EM-TV (Perona-Malik filter-EM-TV), geometric-EM-TV (geometric nonlinear filter-EM-TV), and combined-EM-TV (combined filter-EM-TV). In the TV-steepest descent step, 9 iterations ($=L$) were used with the parameter α set to 0.1 in every step. EM-TV image (Fig. 10b revealed reduced streak artifact shown in EM image (Fig. 10a), but the blocky pattern produced by TV minimization appears on it. Background variability and blocky pattern was considerably reduced when geometric nonlinear filter and the combined

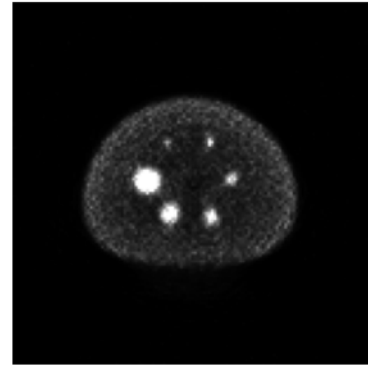


Fig. 9. A slice of the reconstructed IEC phantom images in transaxial view using 120 projections (full samples).

Table 1. Performance of the combined filter in comparison with PM filter and geometric nonlinear filter. (The performance was evaluated with slice 28 from 2D stacks of 3D Torso phantom.)

Image	Pre-filter	NMSE	SI	β	SNR gain
Torso phantom	PM filter	0.5447	0.1068	0.9756	6.8835
	Geometric nonlinear filter	0.6982	0.1829	0.9713	6.0036
	Combined filter	0.5606	0.1156	0.9755	7.1285

filter was applied to projections before reconstruction. Furthermore, compared to geometric-EM-TV, combined-EM-TV preserved edges well and produced a high-contrast image. Figs. 11 and Fig. 12 show quantitative measurements of CNR and uniformity for the reconstructed images. For the spheres with large diameters, the combined filter showed CNR value greater than geometric nonlinear filter while geometric nonlinear filter produced the highest uniformity.

DISCUSSION

In order to reduce CT radiation dose while enhancing the image quality, accurate image reconstruction from few-views in divergent-beam CT was proposed in ref. [9]. However, this method, known as TV image reconstruction method, produces undesirable errors and artifacts such as systematic loss of contrast [15] and blocky artifacts when applied to the

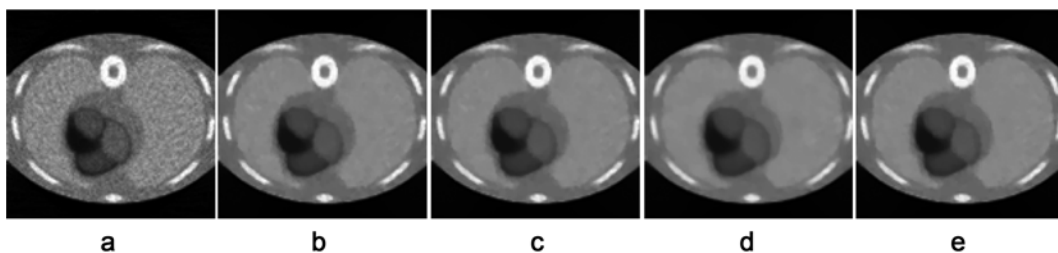


Fig. 8. The reconstructed images using (a) EM and (b) EM-TV from the sparse sinogram in Fig. 5b without applying pre-filters, and the images reconstructed from filtered projection data using (c) PM filter, (d) geometric nonlinear filter, and (e) the combined filter.

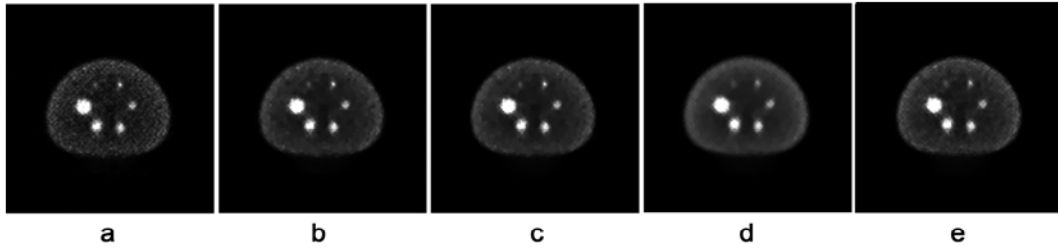


Fig. 10. Images reconstructed from the sparse view data with 50% angular samples (60 projections) using (a) EM, (b) EM-TV, (c) PM-EM-TV, (d) geometric-EM-TV, and (e) combined-EM-TV.

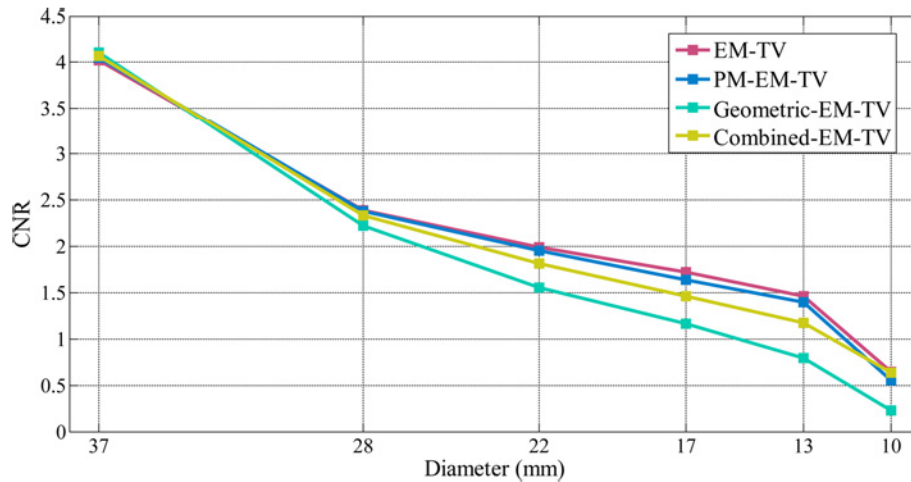


Fig. 11. Quantitative measurements of CNR for the reconstructed images in Fig. 10.

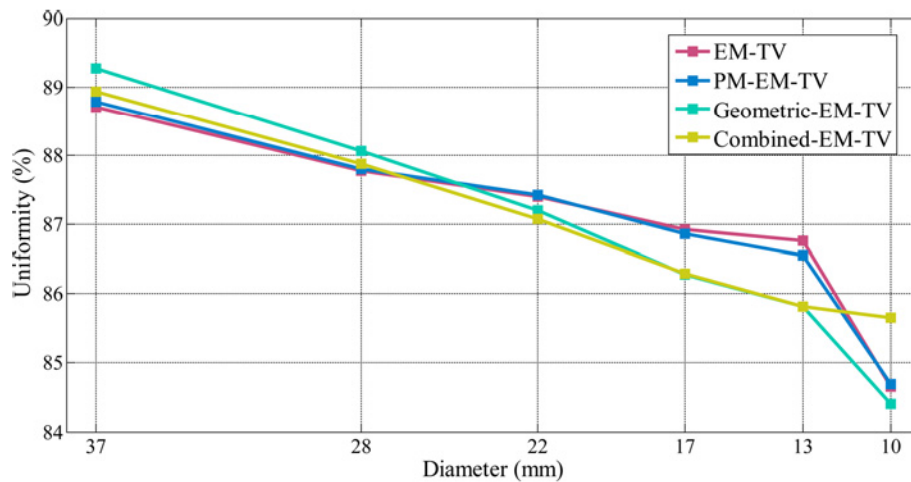


Fig. 12. Quantitative measurements of uniformity for the reconstructed images in Fig. 10.

noisy data. To reduce such effects, we applied various diffusion filters to the projection data as a pre-filter and also proposed the combined filter in this study.

In the numerical simulation, we first explored the convergence property of the combined filter and compare it with that of other filters using SL phantom. As the number of iterations got higher, NMSE value of noisy phantom image decreased rapidly and the lowest NMSE value was

obtained by use of combined filter. This proved that combining two diffusion filters was effective in reducing noise. Next, we evaluated the combined filter as a pre-filter for SPECT image reconstruction of reduced angular sampled data using 3D digital torso phantom. The experiments using the 3D torso phantom proved that the combined filter has characteristics that lie somewhere between those of PM filter and geometric nonlinear filter. In other words, it is suitable

for noise reduction while preserving edges.

In the real IEC phantom experiment, improvements in CNR and uniformity were quantitatively measured for the proposed method and compared with EM-TV, PM-EM-TV and geometric-EM-TV. The proposed method improved uniformity while maintaining CNR and reducing blocky pattern compared to EM-TV. On the other hand, geometric-EM-TV appears to produce the lowest CNR. Therefore, it can be deduced that it is important to preserve edges when reducing noise in the sinogram domain before the TV reconstruction for maintaining contrast of lesion in reconstructed images. This is consistent with the results in ref. [16], where anisotropic adaptive filtering was applied to the projection data for noise reduction in cone beam CT. The combined filter can also be used as a post-filter after image reconstruction. However, post-filtering methods were not effective since the noise propagates through the reconstruction.

Using diffusion filters as a pre-filter in the projection domain can reduce artifacts originated from the TV reconstruction when applied to the noisy data. As a consequence, the images can be reconstructed using the TV method with reduced systematic loss of contrast and blocky artifacts when angular sampling is low. This can lower the patient exposure to radiation due to high radiation dose or long scan time. In this study, EM-TV with the combination of PM and geometric nonlinear diffusion filters was found to improve uniformity while maintaining CNR when angular sampling is low. In conclusion, the TV image reconstruction combined with the proposed diffusion filter can be beneficial for clinical SPECT imaging by reducing scan time.

ACKNOWLEDGMENTS

This work was supported by grants from Seoul National University Hospital (0420130600 (2013-1192)), National Research Foundation of Korea (NRF) funded by the Korean Ministry of Science, ICT and Future Planning (NRF-2013R1A2A1A05006227), and Korea Healthcare Technology R&D Project, Ministry of Health & Welfare, Republic of Korea (H113C01630200).

CONFLICT OF INTEREST STATEMENTS

Son J declares that she has no conflict of interest in relation to the work in this article. Kim SM declares that she has no conflict of interest in relation to the work in this article. Lee

JS declares that he has no conflict of interest in relation to the work in this article.

REFERENCES

- [1] So Y, Lee HY, Kim SK, Lee JS, Wang KC, Cho BK, Kang E, Lee DS. Prediction of the clinical outcome of pediatric moyamoya disease with postoperative basal/acetazolamide stress brain perfusion SPECT after revascularization surgery. *Stroke*. 2005; 36(7):1485-9.
- [2] de Jong HWAM, Boellaard R, Knoess C, Lenox M, Michel C, Casey M, Lammertsma AA. Correction methods for missing data in sinograms of the HRRT PET scanner. *IEEE T Nucl Sci*. 2003; 50(5):1452-6.
- [3] Karp JS, Muehllehner G, Lewitt RM. Constrained Fourier space method for compensation of missing data in emission computed tomography. *IEEE T Med Imaging*. 1988; 7(1):21-5.
- [4] Tuna U, Peltonen S, Ruotsalainen U. Gap-filling for the high-resolution PET sinograms with a dedicated DCT-domain filter. *IEEE T Med Imaging*. 2010; 29(3):830-9.
- [5] Kinahan PE, Fessler JA, Karp JS. Statistical image reconstruction in PET with compensation for missing data. *IEEE T Nucl Sci*. 1997; 44(4):1552-7.
- [6] Nguyen V-G, Lee S-J. Image reconstruction from limited-view projections by convex nonquadratic spline regularization. *Opt Eng*. 2010; 49(3):037001.
- [7] Choi K, Wang J, Zhu L, Suh TS, Boyd S, Xing L. Compressed sensing based cone-beam computed tomography reconstruction with a first-order method. *Med Phys*. 2010; 37(9):5113-25.
- [8] Pan X, Sidky EY, Vannier M. Why do commercial CT scanners still employ traditional, filtered back-projection for image reconstruction? *Inverse Probl*. 2009; 25(12):1-36.
- [9] Sidky EY, Pan X. Image reconstruction in circular cone-beam computed tomography by constrained, total-variation minimization. *Phys Med Biol*. 2008; 53(17):4777-807.
- [10] Ahn S, Kim SM, Son J, Lee DS, Lee JS. Gap compensation during PET image reconstruction by constrained, total-variation minimization. *Med Phys*. 2012; 39(2):589-602.
- [11] Michel-Gonzalez E, Cho MH, Lee SY. Geometric nonlinear diffusion filter and its application to X-ray imaging. *Biomed Eng Online*. 2011; doi: 10.1186/1475-925X-10-47.
- [12] Perona P, Malik J. Scale-space and edge detection using anisotropic diffusion. *IEEE T Pattern Anal*. 1990; 12(7):629-39.
- [13] Jin SO, Kim JG, Lee SY, Kwon O-K. Bone-induced streak artifact suppression in sparse-view CT image reconstruction. *Biomed Eng Online*. 2012; doi: 10.1186/1475-925X-11-44.
- [14] Sattar F, Floreby L, Salomonsson G, Lövström B. Image enhancement based on a nonlinear multiscale method. *IEEE T Image Process*. 1997; 6(6):888-95.
- [15] Meyer Y. *Oscillating Patterns in Image Processing and Nonlinear Evolution Equations: The Fifteenth Dean Jacqueline B. Lewis Memorial Lectures*. 1st ed. Providence: American Mathematical Society; 2001.
- [16] Maier A, Wigstrom L, Hoffmann HG, Homegger J, Zhu L, Strobel N, Fahrig R. Three-dimensional anisotropic adaptive filtering of projection data for noise reduction in cone beam CT. *Med Phys*. 2011; 38(11):5896-909.